Turbulence, Heat and Mass Transfer 7

Structural LES modeling using a high-order spectral difference scheme for unstructured meshes

G. Lodato, P. Castonguay and A. Jameson

Department of Aeronautics & Astronautics, Stanford University,
Durand Building, 496 Lomita Mall, Stanford, CA 94305-4035, glodato@stanford.edu

Abstract — The combination of the high-order unstructured Spectral Difference (SD) spatial discretization scheme with Sub-Grid Scale (SGS) modeling for Large-Eddy Simulation (LES) was investigated with particular focus on the implementation of similarity mixed formulations. A new class of constrained discrete filters to be used with the SD scheme were developed. The novel discrete filters can be applied to any SGS model involving explicit filtering and to a broad class of high-order discontinuous Finite Element (FE) numerical schemes. The code was validated on turbulent channel flow at different Reynolds numbers, and results were compared against Direct Numerical Simulation (DNS). The numerical experiments suggest that the results are sensitive to the use of the SGS model, even when high-order numerical schemes are used, especially when the grid resolution is kept relatively low, and mostly in terms of resolved Reynolds stresses. The use of a simple wall-modeling strategy in conjunction with the SGS model is also reported.

1. Introduction

Notwithstanding the considerable effort which has been devoted to the development of accurate and relatively reliable SGS models for LES, in most cases, the underlying numerical methods rely upon highly dissipative schemes. The inherent numerical dissipation introduced by such numerical schemes limits their ability to represent the spectrum resolved in LES. Hence it is necessary to combine high order numerical schemes with advanced SGS modeling techniques in order for LES to become a valuable and reliable tool for fundamental flow physics and industrial applications. Unfortunately, most of the available high-order numerical schemes are designed to be used on cartesian or very smooth structured curvilinear meshes and therefore they are inadequate to simulate turbulent flows over complex geometries. In the current work, a high-order unstructured mesh solver is combined with an explicit filtering LES method, thus allowing highly accurate turbulent flow computations on realistic geometries.

High-order numerical schemes for solving the compressible Navier-Stokes equations on unstructured grids have been widely studied during the last decade. By far the most mature and widely used of these schemes are based on the Discontinuous Galerkin (DG) method [1, 2]. Recently, however, several alternative high-order methods have been proposed, including SD type schemes [3–5] , which potentially offer increased efficiency compared with DG methods. It is worthwhile mentioning that it has recently been demonstrated that, for the case of 1D linear advection, both SD and nodal DG type schemes can be formulated within a unifying Flux Reconstruction (FR) framework [6–10]. Such a unifying framework is efficient, straightforward to implement, and allows direct comparisons to be made between various SD and DG methods. The SD method has been successfully applied to viscous compressible flows with shocks [11], implicit LES of turbulent channel flow [12] and flow around circular cylinders [13], as well as, transitional flows over an SD7003 airfoil [14]. The combination of the SD method with SGS modeling techniques for explicit LES, on the other hand, has not been widely studied.

In the context of the SD method for 3D unstructured hexahedral grids, the present study addresses the implementation of a structural SGS model based on the scale similarity assumption [15], with some preliminary results regarding the use of a simple wall-modeling approach.

2. Mathematical formulation

2.1. The numerical scheme

In the present work, the Navier-Stokes equations are solved using the high-order unstructured SD method for spatial discretization. The formulation of the equations on hexahedral grids is similar to the formulation by Sun *et al.* [16], which will be summarized below for completeness. After introducing the *bar* filter operator and the density-weighted Favre filter operator *tilde*, the unsteady compressible Navier-Stokes equations in conservative form are written as

$$\frac{\partial \overline{\boldsymbol{U}}}{\partial t} + \frac{\partial \overline{\boldsymbol{F}}^k}{\partial x_k} = \boldsymbol{0}, \tag{1}$$

where $\overline{\boldsymbol{U}} = \begin{pmatrix} \overline{\rho} & \overline{\rho u_1} & \overline{\rho u_2} & \overline{\rho u_3} & \overline{\rho e} \end{pmatrix}^{\mathrm{T}}$ is the vector of conservative variables, and $\overline{\boldsymbol{F}}^k = \overline{\boldsymbol{F_I}}^k - \overline{\boldsymbol{D}}^k$ accounts for the inviscid and viscous flux vectors, which are defined as

$$\overline{\boldsymbol{F_I}}^k = \begin{pmatrix} \overline{\rho u}_k \\ \overline{\rho u}_1 \widetilde{u}_k + \delta_{1k}\overline{\varpi} \\ \overline{\rho u}_2 \widetilde{u}_k + \delta_{2k}\overline{\varpi} \\ \overline{\rho u}_3 \widetilde{u}_k + \delta_{3k}\overline{\varpi} \\ (\overline{\rho e} + \overline{\varpi})\widetilde{u}_k \end{pmatrix}, \quad \overline{\boldsymbol{D}}^k = \begin{pmatrix} 0 \\ 2\overline{\mu}\widetilde{A}_{1k} + \tau^{\mathrm{d}}_{1k} \\ 2\overline{\mu}\widetilde{A}_{2k} + \tau^{\mathrm{d}}_{2k} \\ 2\overline{\mu}\widetilde{A}_{3k} + \tau^{\mathrm{d}}_{3k} \\ 2\overline{\mu}\widetilde{u}_j \widetilde{A}_{kj} + \frac{\overline{\mu} c_p}{\boldsymbol{Pr}} \frac{\partial \widetilde{\vartheta}}{\partial x_k} + q_k \end{pmatrix}, \tag{2}$$

where ρ is the fluid's density, u_k is the velocity vector, e is the total energy (internal + kinetic), μ is the dynamic viscosity, A_{ij} is the deviator of the deformation tensor, c_p is the specific heat capacity at constant pressure and $\boldsymbol{Pr}$ is the Prandtl number. In particular, $\overline{\varpi}$ and $\widetilde{\vartheta}$ are the filtered *macro-pressure* and *macro-temperature* [15, 17], these quantities being related by the usual equation of state, *i.e.*, $\overline{\varpi} = \overline{\rho} R \widetilde{\vartheta}$. τ_{ij} and q_k in Eq. (2) represent the usual unclosed SGS terms (note that the superscript 'd' refers to the deviatoric part of the relevant tensor).

To achieve an efficient implementation, all elements in the physical domain are transformed to a standard cubic element described by local coordinates $\boldsymbol{\xi} = (\xi_1, \xi_2, \xi_3)$, with $\boldsymbol{\xi} \in [0 : 1]^3$. The governing equations in the physical domain are then transferred into the computational domain, and they take the form

$$\frac{\partial \overline{\boldsymbol{\mathcal{U}}}}{\partial t} + \frac{\partial \overline{\boldsymbol{\mathcal{F}}}^k}{\partial \xi_k} = \boldsymbol{0}, \tag{3}$$

where

$$\overline{\boldsymbol{\mathcal{U}}} = |\det(\mathsf{J})| \overline{\boldsymbol{U}} \quad \text{and} \quad \overline{\boldsymbol{\mathcal{F}}}^k = |\det(\mathsf{J})| \frac{\partial \xi_k}{\partial x_j} \overline{\boldsymbol{F}}^j, \tag{4}$$

and $\det(\mathsf{J})$ represents the determinant of the Jacobian matrix $\mathsf{J}_{ij} = \partial x_i / \partial \xi_j$.

In order to construct a degree $(N-1)$ polynomial for each coordinate direction, solution at N points are required. These N points in 1D are chosen to be the Gauss-Legendre quadrature points, whereas the flux points were selected to be the Gauss-Legendre quadrature points of order $N-1$ plus the two end points 0 and 1. Using the N solution points and the $N+1$ flux

points, polynomials of degree $N-1$ and N, respectively, can be built using Lagrange bases defined as

$$h_i(\xi) = \prod_{s=1,s\neq i}^{N} \left(\frac{\xi-\xi_s}{\xi_i-\xi_s}\right), \quad \text{and} \quad l_{i+1/2}(\xi) = \prod_{s=0,s\neq i}^{N} \left(\frac{\xi-\xi_{s+1/2}}{\xi_{i+1/2}-\xi_{s+1/2}}\right). \tag{5}$$

The reconstructed solution for the conserved variables in the standard element is then obtained as the tensor product of the three one-dimensional polynomials,

$$\overline{\boldsymbol{U}}(\boldsymbol{\xi}) = \sum_{k=1}^{N}\sum_{j=1}^{N}\sum_{i=1}^{N} \frac{\overline{\boldsymbol{U}}_{i,j,k}}{|J_{i,j,k}|} h_i(\xi_1)h_j(\xi_2)h_k(\xi_3), \tag{6}$$

where i, j and k are the indices of the solution points within each standard element. A similar reconstruction is adopted for the resolved fluxes $\overline{\boldsymbol{\mathcal{F}}}^k$.

The reconstructed fluxes are only element-wise continuous, but discontinuous across cell interfaces. For the inviscid flux, a Riemann solver is employed to compute a common flux at cell interfaces to ensure conservation and stability. In the current implementation, the Roe solver [18] with entropy fix [19] was used. The left and right states here represent the solution on both sides of the shared edge flux point. The viscous flux is a function of both the conserved variables and their gradients, therefore, the solution gradients have to be calculated at the flux points. The average approach described by Sun *et al.* [16] is used to compute the viscous fluxes.

2.2. LES modeling approach

In order to close the SGS terms a structural model based on the scale similarity assumption [20–23] is adopted. In the perspective of developing a similarity mixed formulation [23–30] with correct near-wall scaling, a WALE formulation [31] for the eddy-viscosity term was recently proposed by Lodato *et al.* [15]:

$$\tau_{ij}^{\mathrm{d}} = 2\overline{\rho}\nu_{\mathrm{sgs}}\widetilde{A}_{ij} - \overline{\rho}\big(\widehat{\widetilde{u}_i\widetilde{u}_j} - \widehat{\widetilde{u}}_i\widehat{\widetilde{u}}_j\big)^{\mathrm{d}}, \tag{7}$$

$$q_k = \gamma\overline{\rho}\kappa_{\mathrm{sgs}}\frac{\partial\widetilde{e_I}}{\partial x_k} - \gamma\overline{\rho}\big(\widehat{\widetilde{e_I}\widetilde{u}_k} - \widehat{\widetilde{e}}_I\widehat{\widetilde{u}}_k\big), \tag{8}$$

where $\widetilde{e_I}$ is the resolved internal energy and the *hat* operator represents filtering at cutoff length $\alpha\Delta_{\mathrm{g}}$, where Δ_{g} is a measure of the actual grid resolution (see below), and $\alpha \geq 1$ with sufficient localization in physical space [22]. the SGS kinematic viscosity, ν_{sgs}, and thermal diffusivity, κ_{sgs}, are computed as [31]

$$\nu_{\mathrm{sgs}} = C_{\mathrm{w}}^2\Delta_{\mathrm{g}}^2\frac{(\widetilde{s}_{ij}^{\mathrm{d}}\widetilde{s}_{ij}^{\mathrm{d}})^{3/2}}{(\widetilde{A}_{ij}\widetilde{A}_{ij})^{5/2} + (\widetilde{s}_{ij}^{\mathrm{d}}\widetilde{s}_{ij}^{\mathrm{d}})^{5/4}}, \quad \text{and} \quad \kappa_{\mathrm{sgs}} = \frac{\nu_{\mathrm{sgs}}}{Pr_{\mathrm{sgs}}}, \tag{9}$$

where $C_{\mathrm{w}} = 0.5$, and $\widetilde{s}_{ij}^{\mathrm{d}}$ is the traceless symmetric part of the square of the resolved velocity gradient tensor $\widetilde{g}_{ij} = \partial\widetilde{u}_i/\partial x_j$. The sub-grid scale Prandtl number, Pr_{sgs}, is assumed constant and equal to 0.5. [28, 30], and Δ_{g} is computed from its counterpart in computational space, namely $\Delta = 1/N$, following the same procedure suggested by Parsani *et al.* [32]:

$$\Delta(\boldsymbol{\xi}) \sim \left[\frac{|\det(\mathsf{J}(\boldsymbol{\xi}))|}{N^3}\right]^{1/3} = \Delta|\det(\mathsf{J}(\boldsymbol{\xi}))|^{1/3}. \tag{10}$$

2.3. Constrained discrete filters for the SD method

When using similarity mixed SGS models, such as the WSM model used in this study, explicit filtering represents a key ingredient to approximate sub-grid scale interactions. This is done by assuming similarity within a narrow band of frequencies in the vicinity of the cutoff frequency. Similarity is assumed between the SGS scales and the smallest resolved scales, which are evaluated as the difference between the filtered and the twice-filtered field. Hence, the explicit filter should be designed (a) to have sufficient localization in physical space; (b) to ensure a certain selected cutoff length-scale. In the present study, sufficient localization in physical space is achieved by setting $\Delta_{\mathrm{c}} = 1.5\Delta$.

In order to develop a mixed similarity formulation to be applied with the SD method, the above ideas need to be generalized in a way which is numerically consistent with the use of SD elements. In particular, since the SGS model terms are evaluated at the flux points, the filtered quantities needs to be evaluated at the same flux points starting from the discrete solution at the solution points. This can be achieved by filtering the solution at the solution points first, and then extrapolating the filtered quantities at the flux points using the same Lagrange polynomials used to reconstruct the fluxes (*cf.* Eq. (5)). A particularly desirable feature in building discrete filters is that the filter stencil does not lie across elements. Moreover, the non-uniform spacing of the solution points should be taken into account. The above considerations lead to the particularly challenging task of designing asymmetric non-uniform discrete filters with a fixed cutoff length-scale.

For the 1D SD element, the discrete filter for a generic quantity ϕ is defined as [33]

$$\overline{\phi}_s = \sum_{i=1}^{N} w_i^s \phi_i, \quad (s = 1, \ldots, N), \tag{11}$$

where the s index refers to a quantity at the N solution points. For the case of hexahedral elements as in the present study, the generalization to three dimensions follows immediately by tensor product of 1D filtering operators. The spectral signature of the above discrete filter is characterized by its transfer function in Fourier space [34], which is readily obtained as

$$\widehat{G}_s(k) = \sum_{i=1}^{N} w_i^s \exp(-\mathrm{j}\beta_i^s k\Delta), \quad \text{with} \quad \beta_i^s = \frac{\xi_i - \xi_s}{\Delta}, \tag{12}$$

where k is the wavenumber and $\mathrm{j} = \sqrt{-1}$; ξ_s represents the location of the solution points, whereas $\Delta = 1/N$ is assumed to be the actual resolution within the SD element (*cf.* Eq. (10)).

A possible strategy to build discrete filters can be devised by exploiting the resolution properties of polynomials of different order, thus performing the explicit filtering operation by applying the Restriction-Prolongation (RP) technique in each computational cell [11, 35]. Based on Eq. (12), for instance, the real part of the Fourier transform of the discrete filters constructed using the Restriction-Prolongation (RP) technique [11] for $N = 3$ and 4 is plotted in figure 1(a, d), where the Gaussian filter, with cutoff length equal to 1.5Δ, is also represented for reference. As it is immediately evident, the cutoff frequency for each solution point is different and thus the overall effective cutoff frequency is unpredictable. Furthermore, for $N = 4$, the most asymmetric filters have a relatively pronounced over-shoot in the low frequency range, a feature which may lead to non-physical growth of energy. [33]

In order to overcome these problems, two sets of constrained filters have been developed. One of these sets of filters (CD1) features strict positivity but is only applicable to standard elements with a specific distribution of solution points, whereas the other set (CD2) can be applied to arbitrary distributed points. Both sets of discrete filters are completely local inside the standard element, therefore they are straightforward to implement in a parallel environment.

2.3.1. CD filters by Gauss quadrature integration (CD1)

By exploiting the properties of the Gauss-Legendre quadrature points, a discrete filter can be obtained by analytical integration of a selected filter kernel. In particular, the 1D discrete filter is obtained under the assumption that the convolution integral can be approximately restricted within the SD element

$$\overline{\phi}(\eta) = \int_{-\infty}^{+\infty} \phi(\xi) G_\Delta(\eta - \xi) \mathrm{d}\xi \simeq \sum_{i=1}^{N} w_i^{\mathrm{G}} \phi_i G_\Delta(\eta - \xi_i), \tag{13}$$

where G_Δ is the convolution kernel associated with the filter operation at cutoff length Δ, and w_i^{G} are the Gaussian quadrature weights associated with the N solution points ξ_i. Choosing the Gaussian filter [36], the discrete filter weights are immediately obtained as

$$w_i^s = K w_i^{\mathrm{G}} \exp\left[-\gamma(\beta_i^s/\alpha_s)^2\right], \tag{14}$$

where γ is generally taken to be equal to 6, β_i^s is given by Eq. (12), K is a normalization coefficient and $\alpha_s\Delta$ is the desired cutoff length scale. Since the Gauss quadrature weights are strictly positive, the resulting filter weights are all positive as well, thus making this filter particularly well behaved for numerical simulations. The parameter α_s, in particular, is iteratively determined beforehand for each of the N solution points, such that the estimate of the actual cutoff length of the filter based on the second order moment of the filter kernel [37, 38] is as close as possible to the selected value of $\alpha_0 = 1.5$. Finally, the normalization coefficient is computed such that the preservation of a constant property is satisfied, *viz.* $\sum_{i=1}^{N} w_i^s = 1$. The real part of the kernels of CD1 filters for SD elements of order 3 to 6 are plotted in figure 1(b, e).

2.3.2. CD filters for arbitrarily distributed points (CD2)

The method used to derive these CD filters is based on the work of Vasilyev *et al.* [33]. In particular, starting from Eq. (12), the N filter weights w_i^s for the s-th solution point can be determined by providing N constraints. More precisely, a first obvious condition is related to the preservation of a constant variable, namely $\sum_{i=1}^{N} w_i^s = 1$. Then, starting from the idea of building filters whose kernels are as close as possible to that characterizing the Gaussian filter of width $\Delta_{\mathrm{c}} = \alpha\Delta$, the condition

$$\mathrm{Re}[\widehat{G}_s(k_{\mathrm{c}})] = \sum_{i=1}^{N} w_i^s \cos(\beta_i^s k_{\mathrm{c}} \Delta) = \exp\left(\frac{-\Delta_{\mathrm{c}}^2 k^2}{4\gamma}\right)\bigg|_{k=k_{\mathrm{c}}} = \exp(-\pi^2/24), \tag{15}$$

is enforced, with $k_{\mathrm{c}} = \pi/\Delta_{\mathrm{c}}$, therefore constraining the relevant cutoff length-scale. The remaining conditions are obtained by constraining the discrete filter to have $N - 2$ vanishing moments, thus achieving formal commutation with difference operators. [33] The real part of the kernels of these CD2 filters for SD elements of order 3 and 4 are plotted in figure 1(c, f).

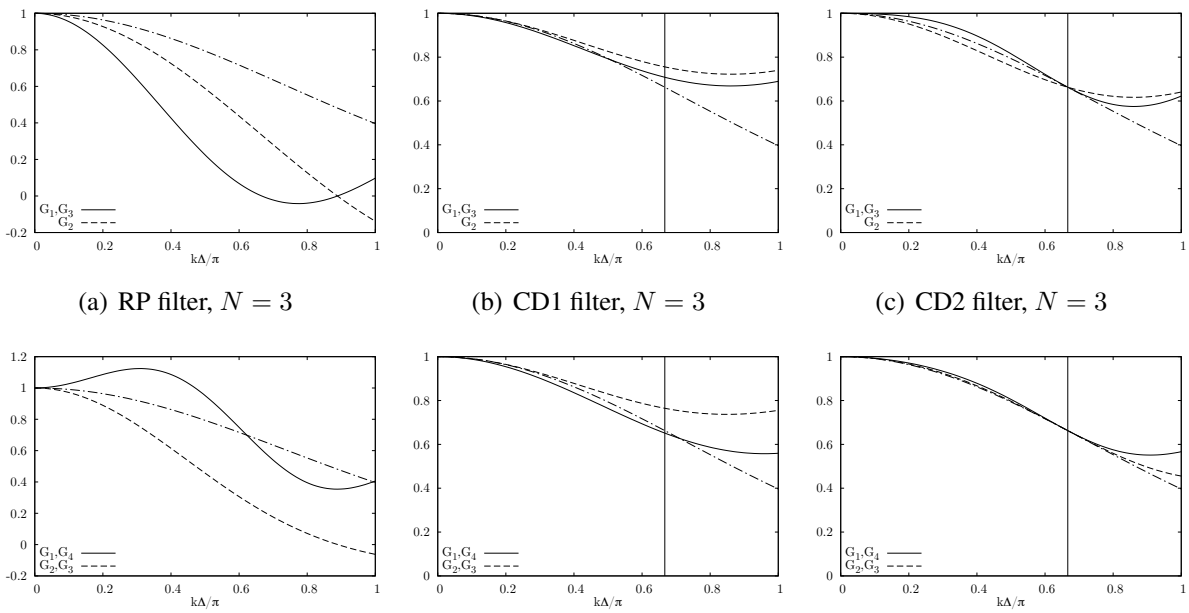

(a) RP filter, $N = 3$ (b) CD1 filter, $N = 3$ (c) CD2 filter, $N = 3$

(d) RP filter, $N = 4$ (e) CD1 filter, $N = 4$ (f) CD2 filter, $N = 4$

Figure 1: Real part of the transfer function $\widehat{G}(k\Delta/\pi)$ of RP (a, d), CD1 (b, e) and CD2 (c, f) filters for different SD discretization orders N (—·— , analytical Gaussian filter).

Re_τ	Re_c	$L_x \times L_y \times L_z$	$n_x \times n_y \times n_z$	N	DoF	Δ_x^+	Δ_y^+	Δ_z^+
180	3 440	$4\pi\delta \times 2\delta \times 2\pi\delta$	$12 \times 12 \times 12$	5	216 000	38	2.0–10	19
395	8 106	$2\pi\delta \times 2\delta \times 1\pi\delta$	$13 \times 9 \times 9$	5	131 625	38	2.1–33	28
590	12 686	$4\pi\delta \times 2\delta \times 1\pi\delta$	$20 \times 12 \times 12$	6	622 080	62	3.4–33	26
590*	12 686	$2\pi\delta \times 2\delta \times 1\pi\delta$	$18 \times 8 \times 8$	5	144 000	46	19.6–38	46
2 000*	48 958	$2\pi\delta \times 2\delta \times 1\pi\delta$	$32 \times 16 \times 16$	5	1 024 000	79	17.8–82	79

Table 1: Grid size and resolution for channel flow computations (resolution is estimated as the element size divided by the number of solution points; DoF = Degrees of Freedom).

3. Results

The behavior of the new discrete filter operators, with the WALE similarity mixed model and the SD method at different orders, is assessed in the following sections on the turbulent channel flow at $Re_\tau = 180$, 395 and 590 (based on the friction velocity u_τ and channel half-width δ) in the case of wall-resolved LES, and at $Re_\tau = 590$ and 2 000 in the case of a (preliminary) attempt of wall-modeled LES. Results are validated against DNS data [39, 40]. All computations were performed at Mach number 0.3, which is low enough to allow comparison with incompressible DNS [41]. Grid dimensions and resolutions for the computations are summarized in table 1, where the last two rows refer to the wall-modeled computations.

3.1. Wall-resolved channel flow

A first check was done on the behavior of the developed filter operators compared with the existing RP filters. The $Re_\tau = 395$ channel flow was selected as a test bench and computations

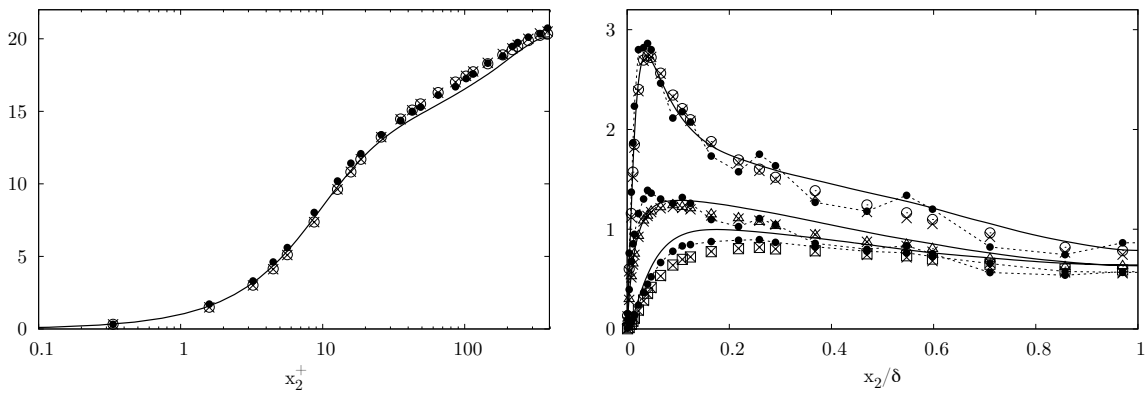

(a) U^+ (b) $u^+_{\rm rms}$, $v^+_{\rm rms}$, $w^+_{\rm rms}$

Figure 2: Mean velocity (a) and RMS of velocity fluctuations (b) for the channel flow at $Re_\tau = 395$, using the SD scheme ($N = 4$) and the WSM model [15]: ○ , LES with CD1 filter; ×, LES with CD2 filter; • LES with RP filter [11]; solid lines, DNS data [39]. ○ , $u^+_{\rm rms}$; □ , $v^+_{\rm rms}$; △ , $w^+_{\rm rms}$.

were performed using the SD scheme with order 4 and the WSM model, where the similarity term was computed using CD1, CD2 and RP filters. The relevant results are shown in figure 2. Although results obtained with different filters are similar in trends, the computation performed with the RP filters shows unphysical numerical oscillations, which are particularly evident on the second-order moments. These numerical artifacts appear to be located at the elements interfaces, and are supposedly strictly related with the over-shoots observed in the kernel of the filters which are applied at those locations (see figure 1(d)). Both CD1 and CD2 filters are numerically better behaved, and the relevant results are almost indistinguishable, proving that these filters provide a complete set of discrete operators to be used with a broad range of high-order discontinuous Finite Elements (FE) methods.

Results from computations performed with the WSM model using the CD1 filter are compared against implicit LES (*i.e.* without SGS model) for the three mentioned Reynolds number in figure 3. For reference, DNS data [39] are plotted as well. In terms of average profiles, the improvement resulting from using the SGS model is marginal. All the plots show good agreement with DNS. The use of the SGS model lead to a slightly better agreement on the intercept of the logarithmic region, which is more evident at $Re_\tau = 180$ and 395. Reynolds stresses, and in particular velocity fluctuations, appear to be much more sensitive to the SGS model. The implicit LES results show a marked tendency to overestimate fluctuations, especially close to the wall and in the streamwise direction, for which the peak is over predicted. Better agreement is obtained with the WSM model with the new proposed filter, which performs consistently better at the three Reynolds numbers.

3.2. Wall-modeled channel flow

In order to gauge the behavior of the implemented WSM model with the new discrete filters in the case that wall-modeling approaches are used, a three-layer Law-of-Wall (LoW) [42] was also tested at $Re_\tau = 590$ and 2 000 (see table 1, last two rows). In particular, the LoW was used inside each wall element, where the wall shear stress was evaluated using information from the farthest solution points from the wall. The relevant results are very encouraging (*cf.* figure 4),

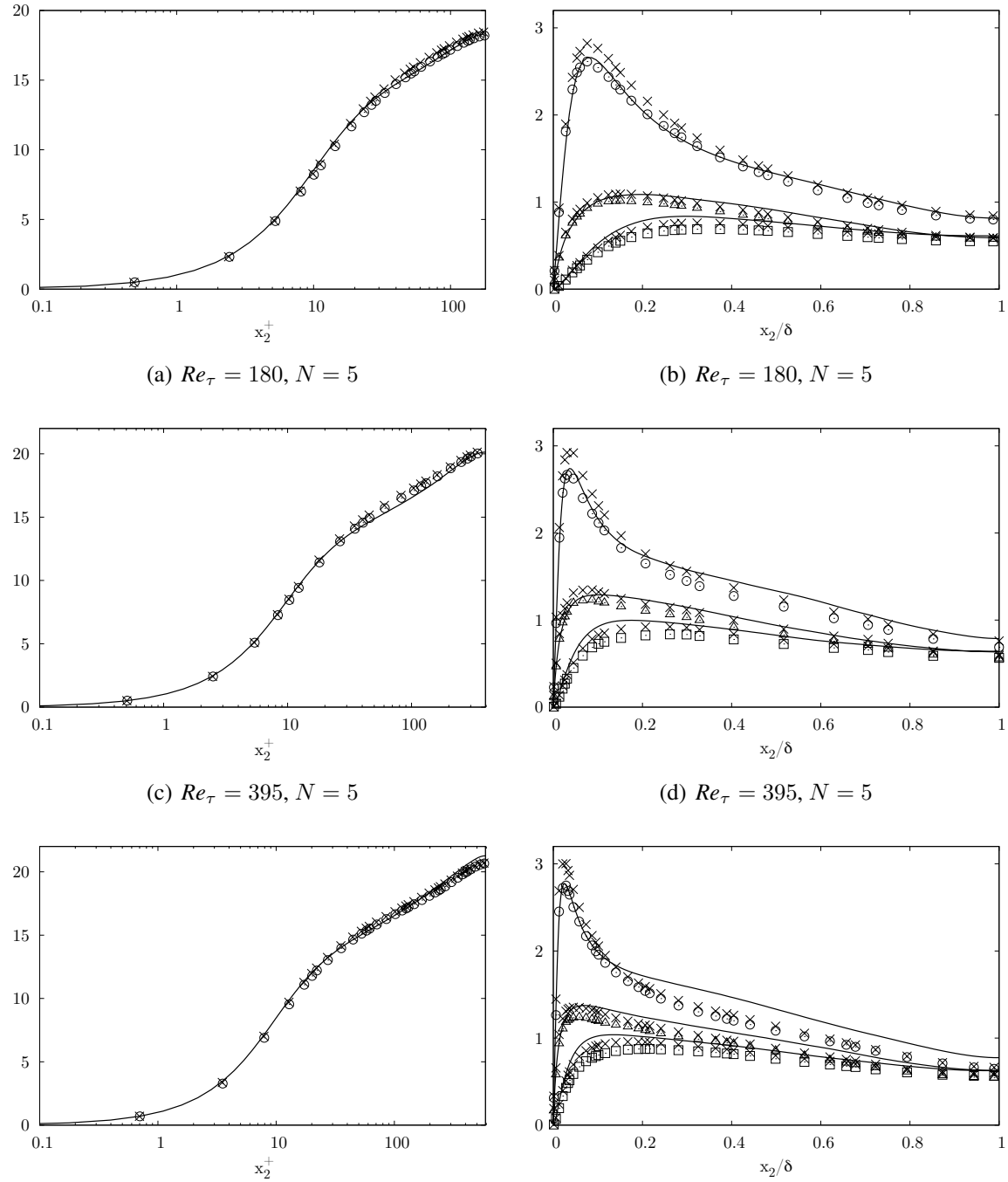

(a) $Re_\tau = 180$, $N = 5$ (b) $Re_\tau = 180$, $N = 5$

(c) $Re_\tau = 395$, $N = 5$ (d) $Re_\tau = 395$, $N = 5$

(e) $Re_\tau = 590$, $N = 6$ (f) $Re_\tau = 590$, $N = 6$

Figure 3: Mean streamwise velocity (a,c,e) and RMS of velocity fluctuations (b,d,f): open symbols, LES with WSM model ($\circ$, U^+ or $u^+_{\rm rms}$; $\square$, $v^+_{\rm rms}$; $\triangle$, $w^+_{\rm rms}$); $\times$, implicit LES; lines, DNS data [39].

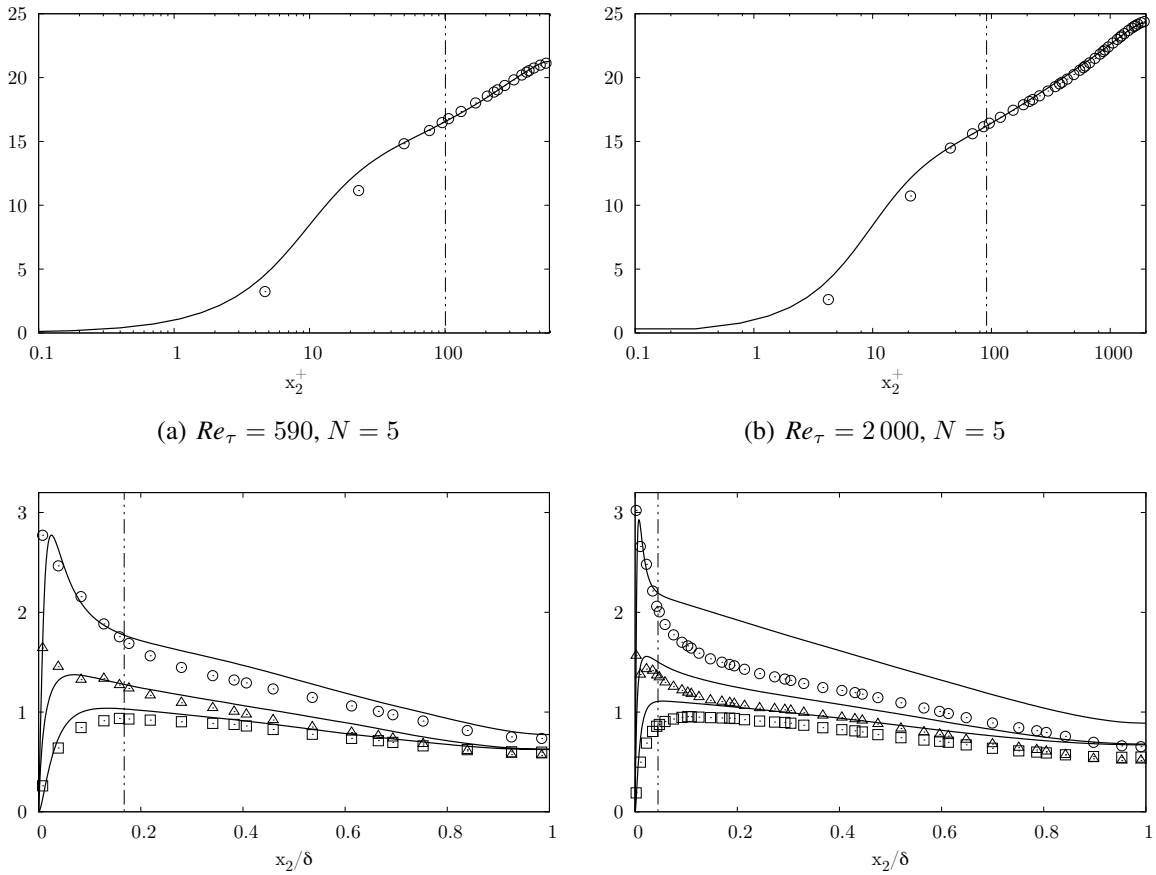

(a) $Re_\tau = 590$, $N = 5$

(b) $Re_\tau = 2\,000$, $N = 5$

(c) $Re_\tau = 590$, $N = 5$

(d) $Re_\tau = 2\,000$, $N = 5$

Figure 4: Mean streamwise velocity (a,b) and RMS of velocity fluctuations (c,d): open symbols, LES with WSM model and law-of-wall (○ , U^+ or $u^+_{\rm rms}$; ▫ , $v^+_{\rm rms}$; △ , $w^+_{\rm rms}$); lines, DNS data [39, 40].

especially in consideration of the simple approach used. Above the modeled region (indicated by a vertical line in the plots), both average profiles and Reynolds stresses are extremely well captured. Even within the modeled region (*i.e.* $x_2^+ < 100$), both computations show the remarkable ability to correctly reproduce trends and peaks of velocity fluctuations (especially in the streamwise direction). As shown in figure. 5, no unphysical numerical artifacts were observed between the LoW modeled layer and the LES resolved region above.

4. Concluding remarks

A similarity mixed model for wall bounded flows was tested in conjunction with the spectral difference scheme. For the similarity mixed formulation used in the present study, in particular, existing filtering approaches based on solution projection over low-order polynomial bases proved to be inadequate, and keen to develop spurious numerical artifacts at the elements interfaces. Hence a new class of discrete filter operators has been developed and tested on the turbulent channel flow at different Reynolds numbers. In the tests performed, the newly developed discrete filters did not lead to any similar unexpected and unphysical behavior throughout the

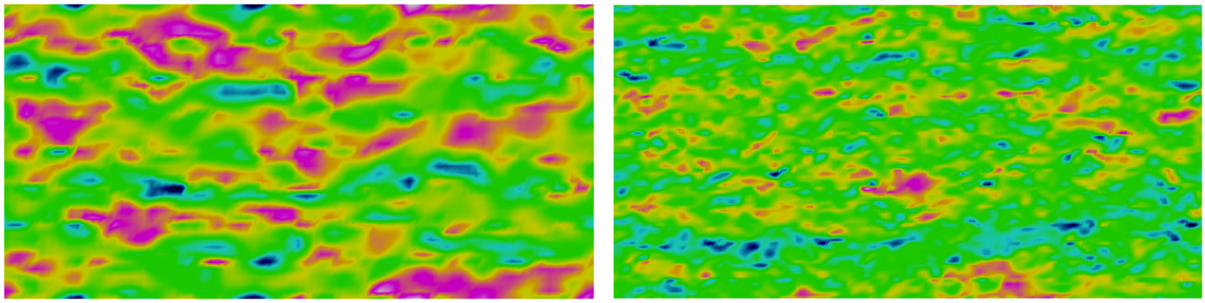

(a) $Re_\tau = 590$ (b) $Re_\tau = 2\,000$

Figure 5: Contours of velocity magnitude over planes at $x_2^+ = 100$ from wall-modeled LES.

computational domain. The proposed constrained discrete filters of arbitrary order, proved to be numerically stable at any tested order (up to $N = 7$ in other tests not included here) and allow a relatively straightforward implementation into high-order SD schemes (or any other discontinuous finite element numerical method) of any SGS model which relies upon the use of explicit filtering or dynamic procedures [43, 44]. Overall, the performance of the SD scheme with the WSM model and the new discrete filters is extremely satisfactory. In the tests performed, the benefits resulting from the use of the model were marginal on the average profiles and more pronounced on the second-order statistical moments. Preliminary tests of wall-modeled LES of channel flow, using an extremely simple three-layers LoW have shown remarkable capabilities to correctly reproduce average profiles and Reynolds stresses even within the modeled region, where turbulent fluctuations are surprisingly well captured in their trends and peaks. The combination of the high-order spectral difference scheme with the SGS modeling approach used in the present study, and the discrete filters developed for this purpose, appears to be a powerful tool for LES of complex geometries.

References

[1] Jan S. Hesthaven and Tim Warburton. *Nodal Discontinuous Galerkin Methods: Algorithms, Analysis, and Applications*. Springer Science+Business Media, LLC, 2008. ISBN 978-0-387-72065-4.

[2] G. Karniadakis and S.J. Sherwin. *Spectral/hp element methods for CFD*. Oxford University Press, USA, 1999.

[3] D.A. Kopriva and J.H. Kolias. A conservative staggered-grid Chebyshev multidomain method for compressible flows. *J. Comput. Phys.*, 125(1):244–261, 1996.

[4] H.T. Huynh. A flux reconstruction approach to high-order schemes including discontinuous Galerkin methods. *AIAA P.*, 2007-4079, 2007. 18th AIAA Computational Fluid Dynamics Conference, Miami, FL, Jun. 25–28, 2007.

[5] H.T. Huynh. A reconstruction approach to high-order schemes including discontinuous Galerkin for diffusion. *AIAA P.*, 2009-403, 2009. 47th AIAA Aerospace Sciences Meeting, Orlando, FL, Jan. 5–8, 2009.

[6] A. Jameson. A proof of the stability of the spectral difference method for all orders of accuracy. *J. Sci. Comput.*, 45(1):348–358, 2010.

[7] P.E. Vincent, P. Castonguay, and A. Jameson. A new class of high-order energy stable flux

reconstruction schemes. *J. Sci. Comput.*, 47(1):1–23, 2010.

[8] A. Jameson, P.E. Vincent, and P. Castonguay. On the non-linear stability of flux reconstruction schemes. *J. Sci. Comput.*, 50(2):434–445, 2012.

[9] P.E. Vincent, P. Castonguay, and A. Jameson. Insights from von Neumann analysis of high-order flux reconstruction schemes. *J. Comput. Phys.*, 230(22):8134–8154, 2011.

[10] P. Castonguay, P.E. Vincent, and A. Jameson. A new class of high-order energy stable flux reconstruction schemes for triangular elements. *J. Sci. Comput.*, 51(1):224–256, 2012.

[11] S. Premasuthan, C. Liang, and A. Jameson. A Spectral Difference method for viscous compressible flows with shocks. *AIAA P.*, 2009-3785, 2009. 19th AIAA Computational Fluid Dynamics, San Antonio, Texas, Jun. 22-25, 2009, 16 p.

[12] C. Liang, S. Premasuthan, A. Jameson, and Z.J. Wang. Large eddy simulation of compressible turbulent channel flow with spectral difference method. *AIAA P.*, 2009-402, 2009. 47th AIAA Aerospace Sciences Meeting Including The New Horizons Forum and Aerospace Exposition, Orlando, FL, Jan. 5–8, 2009, 15 p.

[13] A.H. Mohammad, Z.J. Wang, and C. Liang. Large eddy simulation of flow over a cylinder using high-order spectral difference method. *Adv. Appl. Math. Mech.*, 2(4):451–466, 2010.

[14] P. Castonguay, C. Liang, and A. Jameson. Simulation of Transitional Flow over Airfoils using the Spectral Difference Method. *AIAA P.*, 2010-4626, 2010.

[15] G. Lodato, L. Vervisch, and P. Domingo. A compressible wall-adapting similarity mixed model for Large-Eddy Simulation of the impinging round jet. *Phys. Fluids*, 21(3):035102, 2009.

[16] Y. Sun, Z.J. Wang, and Y. Liu. High-order multidomain spectral difference method for the Navier-Stokes equations on unstructured hexahedral grids. *Commun. Comput. Phys.*, 2(2):310–333, 2007.

[17] Marcel Lesieur, Olivier Métais, and Pierre Comte. *Large-Eddy Simulations of Turbulence*. Cambridge University Press, 2005. ISBN 0-521-78124-8.

[18] P.L. Roe. Approximate Riemann solvers, parameter vectors, and difference schemes. *J. Comput. Phys.*, 43:357–372, 1981.

[19] A. Harten. High resolution schemes for hyperbolic conservation laws. *J. Comput. Phys.*, 49(3):357–393, 1983.

[20] J. Bardina, J.H. Ferziger, and W.C. Reynolds. Improved subgrid-scale models for large-eddy simulation. *AIAA P.*, 1980-1357, July 1980. Fluid and Plasma Dynamics Conference, 13th, Snowmass, CO, Jul. 14-16, 1980, 10 p.

[21] J. Bardina, J.H. Ferziger, and W.C. Reynolds. Improved turbulence models based on LES of homogeneous incompressible turbulent flows. Report TF-19, Thermosciences Division, Dept. Mechanical Engineering, Stanford University, 1984.

[22] S. Liu, C. Meneveau, and J. Katz. On the properties of similarity subgrid-scale models as deduced from measurements in a turbulent jet. *J. Fluid Mech.*, 275:83–119, 1994.

[23] R. Akhavan, A. Ansari, S. Kang, and N. Mangiavacchi. Subgrid-scale interactions in a numerically simulated planar turbulent jet and implications for modeling. *J. Fluid Mech.*, 408:83–120, 2000.

[24] M.V. Salvetti and S. Banerjee. *A priori* tests of a new dynamic subgrid-scale model for finite-difference large-eddy simulations. *Phys. Fluids*, 7(11):2831–2847, November 1995.

[25] R. Anderson and C. Meneveau. Effects of the similarity model in finite-difference LES of isotropic turbulence using a Lagrangian dynamic mixed model. *Flow Turbul. Combust.*,

62(3):201–225, 1999.

[26] T.A. Zang, R.B. Dahlburg, and J.P. Dahlburg. Direct and large-eddy simulations of three-dimensional compressible Navier-Stokes turbulence. *Phys. Fluids A-Fluid*, 4(1):127–140, January 1992.

[27] Yan Zang, Robert L. Street, and Jeffrey R. Koseff. A dynamic mixed subgrid-scale model and its application to turbulent recirculating flows. *Phys. Fluids A-Fluid*, 5(12):3186–3196, December 1993.

[28] G. Erlebacher, M.Y. Hussaini, C.G. Speziale, and T.A. Zang. Toward the large-eddy simulation of compressible turbulent flows. *J. Fluid Mech.*, 238:155–185, 1992.

[29] C.G. Speziale. Galilean invariance of subgrid-scale stress models in the large-eddy simulation of turbulence. *J. Fluid Mech.*, 156:55–62, 1985.

[30] C.G. Speziale, G. Erlebacher, T.A. Zang, and M.Y. Hussaini. The subgrid-scale modeling of compressible turbulence. *Phys. Fluids*, 31(4):940–942, April 1988.

[31] F. Nicoud and F. Ducros. Subgrid-scale stress modelling based on the square of the velocity gradient tensor. *Flow Turbul. Combust.*, 62(3):183–200, September 1999.

[32] M. Parsani, G. Ghorbaniasl, C. Lacor, and E. Turkel. An implicit high-order spectral difference approach for large eddy simulation. *J. Comput. Phys.*, 229(14):5373–5393, 2010.

[33] O.V. Vasilyev, T.S. Lund, and P. Moin. A general class of commutative filters for LES in complex geometries. *J. Comput. Phys.*, 146(1):82–104, 1998.

[34] J. Berland, C. Bogey, O. Marsden, and C. Bailly. High-order, low dispersive and low dissipative explicit schemes for multiple-scale and boundary problems. *J. Comput. Phys.*, 224(2):637–662, 2007.

[35] H.M. Blackburn and S. Schmidt. Spectral element filtering techniques for large eddy simulation with dynamic estimation. *J. Comput. Phys.*, 186(2):610–629, 2003.

[36] Pierre Sagaut. *Large Eddy Simulation for Incompressible Flows: An Introduction*. Springer-Verlag Berlin Heidelberg, 2 edition, 2001. ISBN 3-540-43753-3.

[37] T.S. Lund. On the use of discrete filters for large eddy simulation. In *Annual Research Briefs*, pages 83–95. Center for Turbulence Research, Stanford University, 1997.

[38] A.W. Vreman. The adjoint filter operator in large-eddy simulation of turbulent flow. *Phys. Fluids*, 16(6):2012–2022, 2004.

[39] R.D. Moser, J. Kim, and N.N. Mansour. Direct numerical simulation of turbulent channel flow up to $\mathrm{Re}_\tau = 590$. *Phys. Fluids*, 11(4):943–945, April 1999.

[40] S. Hoyas and J. Jiménez. Scaling of the velocity fluctuations in turbulent channels up to $Re_\tau = 2003$. *Phys. Fluids*, 18:011702, 2006.

[41] H. Foysi, S. Sarkar, and R. Friedrich. Compressibility effects and turbulence scalings in supersonic channel flow. *J. Fluid Mech.*, 509(1):207–216, 2004.

[42] M. Breuer and W. Rodi. Large-eddy simulation of turbulent flow through a straight square duct and a 180 bend. In *Direct and Large-Eddy Simulation I*, pages 273–285. Springer, 1994.

[43] M. Germano, U. Piomelli, P. Moin, and W.H. Cabot. A dynamic subgrid-scale eddy viscosity model. *Phys. Fluids A-Fluid*, 3(7):1760–1765, July 1991.

[44] P. Moin, K. Squires, W. Cabot, and S. Lee. A dynamic subgrid-scale model for compressible turbulence and scalar transport. *Phys. Fluids A-Fluid*, 3(11):2746–2757, November 1991.